Chapter 3

RADIATION TRANSPORT CALCULATIONS FOR HIROSHIMA AND NAGASAKI

Robert T. Santoro, Stephen D. Egbert, John M. Barnes, George D. Kerr, Joseph V. Pace III, James A. Roberts, Charles O. Slater

Introduction

Radiation transport calculations of the neutron and gamma-ray emissions from the atomic bombs detonated at Hiroshima and Nagasaki are presented in this chapter. Neutron emission is classified as prompt and delayed. Prompt neutrons are produced while the weapon is still intact and able to sustain the fission process. Delayed neutrons originate from fission products produced during the fission process. The gamma rays stem from several sources including their production during fission, from reactions of the weapon neutrons in the air, ground and in the weapon itself prior to disassembly, and from fission product decay after disassembly.

The bombs that exploded over Hiroshima and Nagasaki were very different from each other in design and composition. The Hiroshima weapon was the only one of its type ever detonated. In contrast, numerous weapons similar to or the same as the Nagasaki device have been detonated in weapon tests producing a plethora of information that characterize the leakage spectra and other relevant radiation information against which benchmark comparisons of hydrodynamic and radiation transport codes can be made. The Hiroshima weapon leakage radiation characteristics depend primarily on calculations (Chapter 2).

The temporal dependence of neutron and gamma-ray emissions from fission weapons of the types considered in this study is summarized in Table 1 (Kerr et al. 1987). A complete discussion of the calculations to define the leakage spectra from the Hiroshima and Nagasaki weapons is given in Chapter 2. The prompt radiation leakage occurs during the fission process and represents the neutrons and gamma rays that react or pass through the core of the bomb and casing just prior to the explosion and resulting fireball. The characteristics of the leakage spectra depend on the design and composition of the weapon and are obtained from hydrodynamic and radiation transport codes specifically developed for nuclear weapon design and performance assessment. To carry out radiation transport calculations after detonations, it is necessary to have the angle and energy dependent distributions of the prompt neutron and gamma-ray leakage from the weapon. Other parameters needed for these calculations are height of burst and yield. Also

Table 1. Sources of ionizing radiation from nuclear weapons

Sources	Time of emission after detonation
Prompt neutrons from fission	<1 μsec
Delayed neutrons from fission products	<1 min
Prompt gamma rays from the fission process	<1 μsec
Gamma rays from inelastic scattering[a]	
From weapon[b]	<1 μsec
From air	<10 μsec
From surface	<10 μsec
Gamma rays from charged particle reactions[a]	
From weapon[b]	<1 μsec
From air	<10 μsec
From surface	<10 μsec
Capture gamma rays[a]	
From weapon[b]	<1 μsec
From air	Few msec to 0.2 sec
From surface	Few msec to 0.2 sec
Activation gamma rays	
Early times	0.2 sec to 1 min
Residual	1 min to years
Delayed gamma rays from fission products	
Early times	0.2 sec to 1 min
Residual	1 min to years

[a]The gamma rays are of secondary origin and result from interactions of neutrons with air, ground and in the weapon itself.
[b]Included in the source term for neutrons and gamma rays that are emitted while the weapon is still intact and able to sustain the chain reaction.

needed are the compositions of the local environment including the air (density and humidity), ground surface composition including water content and other materials that may have been present at the time of the explosions that would further absorb or scatter the source radiation.

The gamma-ray dose is further categorized in this report as “primary” or “secondary.” The primary gamma-ray dose is obtained from the gamma rays that leak from the weapon and is calculated in Chapter 2. The secondary gamma-ray radiation is obtained from the gamma rays generated by neutron collisions and absorptions in the air, ground, shielding material, or the body itself. Gamma rays generated from air and ground are described in this chapter. Gamma rays generated from shielding material are described in Chapter 7 and Chapter 11. Gamma rays generated from the body are described in Chapter 12.

The following main sections summarize firstly the prompt radiation transport calculations and comparison of results obtained using discrete ordinates methods and Monte Carlo calculations. Second, the delayed neutron and gamma-ray fluence calculations and the procedures to combine these data with the prompt radiation fluences are reviewed. Finally, the calculated DS02 dose and activation data are compared with the same data reported in DS86.

Part A. Prompt Radiation

The prompt radiation transport calculations were performed using an air-over-ground geometry, where the weapon was modeled to detonate over a flat ground surface. For this chapter, the calculation of energy and angular fluences of the air-transported radiation at measurement and survivor locations assumed that (a) the response point was in the open and not shielded by buildings or other structures, (b) the air-ground interface was flat and (c) the ground composition was homogeneous and uniform. The air and ground compositions at the time of the Hiroshima and Nagasaki explosions were the same as in the DS86 Final Report (Kerr et al. 1987). The activation and dosimetry responses for comparison with measured activation and free-field dose were calculated at 1 m above the surface as a function of distance from the hypocenter.

The air-over-ground geometry is highly idealized and, obviously, does not represent the actual landscape-surface environment. No account is made in the prompt radiation calculations for buildings, houses, bridges, terrain variations or other structures that may have affected the behavior and consequences of the radiation or nuclear responses. Analyses to include these effects as well as the effects of topographical features at the two cities are discussed in Chapter 11.

The spatial dependence of the calculated responses may be expressed throughout this document as either a function of ground range or slant range. Slant range is the distance from the epicenter to a response point of interest, where the epicenter is the burst point of the bomb in air. Ground range is the horizontal distance from the hypocenter to a response point of interest, where the hypocenter is the point on the ground directly beneath the epicenter. The ground and slant ranges are the leg and hypotenuse, respectively, of a right triangle given by:

$$(\text{slant range})^2 = (\text{ground range})^2 + (\text{height of burst} - \text{height of response point})^2.$$

Hiroshima and Nagasaki Atmospheric and Surface Conditions

Detailed studies were carried out previously to characterize the atmospheric and ground compositions and conditions at Hiroshima and Nagasaki during the development of DS86.

Meteorology

Kerr et al. (1983, 1987), Tajima (1984), Kerr and Pace (1985), and Tajima et al. (1987) carefully reconstructed the weather conditions at Hiroshima and Nagasaki at the times of the bombings, and Hoshi et al. (1992) recently confirmed the data. At the times of the bombings, the weather in Japan was typically seasonal with light winds and good visibility. High barometric pressure with hot and humid air characteristic of the summer monsoon season prevailed over most of the country. The ground level, burst height and mean atmospheric parameters for the two cities are summarized in Table 2 (Kerr et al. 1987) and the altitude dependent atmospheric profiles for the two cities shown in Table 3 (Kerr et al. 1987). The altitude dependent atmospheric densities for moist air, dry air and water vapor content are given for seven intervals above the ground. Meteorological data are required in the transport calculations to account for attenuation and scattering of the source radiation in transit to the ground and to account for the effects of skyshine.

Table 2. Ground level, burst height and mean atmospheric parameters

Atmospheric parameter	Hiroshima	Nagasaki
Ground Level Values		
Barometric Pressure (mb)[a]	1018.1	1014.0
Air Temperature (°C) [a]	26.7	28.8
Relative Humidity (%)[b]	80	71
Moist Air Density (g cm^{-3})	1.171×10^{-3}	1.158×10^{-3}
Dry Air Density (g cm^{-3})	1.150×10^{-3}	1.137×10^{-3}
Water Vapor Density (g cm^{-3})	2.025×10^{-5}	2.017×10^{-5}
Burst Height Values		
Barometric Pressure (mb)	952.6	957.6
Air Temperature (°C)	22.8	24.6
Relative Humidity (%)	80	71
Moist Air Density (g cm^{-3})	1.111×10^{-3}	1.110×10^{-3}
Dry Air Density (g cm^{-3})	1.095×10^{-3}	1.094×10^{-3}
Water Vapor Density (g cm^{-3})	1.627×10^{-5}	1.600×10^{-5}
Mean Density Values [c]		
Moist Air (g cm^{-3})	1.141×10^{-3}	1.134×10^{-3}
Dry Air (g cm^{-3})	1.123×10^{-3}	1.116×10^{-3}
Water Vapor (g cm^{-3})	1.820×10^{-5}	1.802×10^{-5}

[a]Assumes a temperature lapse rate of 0.67 and 0.83°C per 100 m in Hiroshima and Nagasaki, respectively. The temperatures at the burst heights are estimated to be accurate within ±1°C and the densities of both moist and dry air at burst height are estimated to be accurate within ±0.5% at a 67% confidence level.

[b]Assumes the relative humidity at burst height is the same as at ground level in both Hiroshima and Nagasaki. The relative humidities and densities of water vapor at the burst height are estimated to be accurate within ±5% at a 67% confidence level.

[c]The mean density values for moist and dry air are estimated to be accurate to within ±0.25% and the mean density for water vapor is estimated to be accurate within ±2.5% at a 67% confidence level.

Table 3. Hiroshima and Nagasaki atmospheric density and composition profiles

Air zone	Height (m)	Atmospheric density (g cm^{-3})			Atom density (atom b^{-1} cm^{-1})[a]			
		Moist air	Dry air	Water vapor	H	N	O	Ar
Hiroshima								
Mean	0-500	1.141E-3[b]	1.123E-3	1.820E-5	1.217E-6	3.646E-5	1.039E-5	2.181E-7
1	0-125	1.164E-3	1.144E-3	1.978E-5	1.323E-6	3.715E-5	1.063E-5	2.222E-7
2	125-275	1.150E-3	1.131E-3	1.879E-5	1.256E-6	3.673E-5	1.048E-5	2.196E-7
3	275-449	1.134E-3	1.116E-3	1.768E-5	1.182E-6	3.622E-5	1.031E-5	2.166E-7
4	449-635	1.115E-3	1.099E-3	1.650E-5	1.104E-6	3.567E-5	1.012E-5	2.134E-7
5	635-835	1.096E-3	1.081E-3	1.533E-5	1.025E-6	3.508E-5	9.925E-6	2.098E-7
6	835-1095	1.073E-3	1.059E-3	1.402E-5	9.370E-7	3.439E-5	9.695E-6	2.057E-7
7	1095-2000	1.041E-3	1.029E-3	1.229E-5	8.217E-7	3.340E-5	9.371E-6	1.998E-7
Nagasaki								
Mean	0-500	1.134E-3	1.116E-3	1.802E-5	1.205E-6	3.624E-5	1.032E-5	2.167E-7
1	0-125	1.152E-3	1.132E-3	1.961E-5	1.311E-6	3.676E-5	1.052E-5	2.198E-7
2	125-275	1.139E-3	1.121E-3	1.842E-5	1.231E-6	3.638E-5	1.037E-5	2.176E-7
3	275-449	1.124E-3	1.107E-3	1.709E-5	1.142E-6	3.593E-5	1.021E-5	2.149E-7
4	449-635	1.107E-3	1.091E-3	1.571E-5	1.050E-6	3.543E-5	1.003E-5	2.119E-7
5	635-835	1.089E-3	1.075E-3	1.434E-5	9.590E-7	3.490E-5	9.841E-6	2.087E-7
6	835-1095	1.068E-3	1.055E-3	1.285E-5	8.589E-7	3.426E-5	9.621E-6	2.049E-7
7	1095-2000	1.038E-3	1.027E-3	1.092E-5	7.303E-7	3.335E-5	9.312E-6	1.995E-7

[a]b = barn = 1×10^{-24} cm^2

[b]Read as 1.141×10^{-3}.

Ground and Surface Compositions

The composition of the ground or surface materials significantly affects the initial radiation transport and the activation in and immediately (within a few meters) above the ground. The soil composition has been investigated by both Japan and US research teams. Hashizume et al. (1969) collected fifty samples of soil in Hiroshima during the summer of 1966, analyzed the soil composition for a few chemical elements that were activated by thermal neutrons, and determined the free water content of the fifty samples. The free water content ranged from 25-35% of dry soil and averaged about 30% (Hashizume et al. 1969).

Kerr et al. (1983, 1987) investigated dry soil samples from a couple of undisturbed sites at each of the two cities using both atomic emission spectroscopy and neutron activation analysis. Based on these and other data (Kerr et al. 1987), the dry soil density was assumed to be 1.3 g cm^{-3}, excluding water content but including pore spaces. Typical soils contain approximately 50% dry material and approximately 50% pore spaces that may contain either water or air. The free water concentration in soil is usually expressed in percent and is defined as the water loss from a moist soil sample that has been oven dried at 105 °C divided by the mass of the dry soil materials. Using this criterion, the water density was determined to be 0.4 g cm^{-3} using a mean value of 30% for the free water content and a bulk density of 1.3 g cm^{-3} for dry soil.

The soil compositions used in both the DS86 and DS02 radiation transport calculations are given in Table 4 (Kerr et al. 1983). The atom densities were calculated using an overall ground density of 1.7 g cm^{-3}. More recently data have been found in the United States Strategic Bombing Survey (USSBS) of Hiroshima and Nagasaki that suggests the free water content of the soil may have been less than previously assumed. The USSBS report for Hiroshima (1947a) states there had been practically no rain in the city for 3 weeks prior to the bombing, and the USSBS report for Nagasaki (1947b) states there had been no rain for 10 days prior to August 9, except for one light shower on August 5.

The effect of free water content on the transport of radiation was investigated using the MCNP radiation transport code (Briesmeister 2000), the new neutron source term for Hiroshima, and several different interface materials. The ratios of various nuclear reactions at 1 m above different interface materials to the same reactions at 1 m above wet ground (30% moisture) are compared in Table 5. In damp ground, the moisture content was taken as 15%, and it is zero in the dry ground. The composition and density of dry ground were taken from Kerr et al. (1987), and the composition and density for concrete and granite were taken from Shizuma et al. (1997). The 50-cm thickness of wet ground normally used in the DS02 calculations was simply replaced with 50 cm of the material of interest using the appropriate composition and density.

The ratios in Table 5 were obtained from the MCNP radiation transport calculations between ground ranges of 200 to 1,000 m where the MCNP results were accurate to within 5%. The result for damp ground (15%) is not very different from the normally-used wet ground (maximum of 6% for neutron kerma). Hence, the wet soil used in our DS02 calculations gives reliable results for radiation transport in air-over-ground for the range of free water content that would be normally expected in the soils of either Hiroshima or Nagasaki. The other data for dry soil, concrete, and granite suggests that the effects of the local neutron-scattering environment can be very important when considering neutron activation of building materials or neutron kerma for shielded survivors. Gamma-ray doses from the primary prompt and delayed components are unaffected by the moisture content of the ground. If the ground was recalculated using concrete,

Table 4. Hiroshima and Nagasaki wet ground composition

Chemical composition	Hiroshima		Nagasaki	
	Atom density (atom b^{-1} cm^{-1})[a]	Percent bymass	Atom density (atom b^{-1} cm^{-1})[a]	Percent by mass
H	3.085×10^{-2}	3.04	3.521×10^{-2}	3.47
C	7.043×10^{-4}	0.83	1.806×10^{-3}	2.12
O	3.759×10^{-2}	58.74	3.857×10^{-2}	60.27
Na	5.451×10^{-4}	1.22	2.556×10^{-4}	0.57
Al	2.061×10^{-3}	5.43	2.816×10^{-3}	7.42
Si	9.315×10^{-3}	25.55	6.806×10^{-3}	18.67
Cl	2.541×10^{-6}	0.01	7.512×10^{-6}	0.03
K	7.191×10^{-4}	2.75	1.510×10^{-4}	0.58
Ca	1.583×10^{-4}	0.62	2.267×10^{-4}	0.89
Ti	2.567×10^{-5}	0.12	1.034×10^{-4}	0.48
Mn	6.659×10^{-6}	0.04	1.796×10^{-5}	0.10
Fe	2.482×10^{-4}	1.35	8.247×10^{-4}	4.50

[a] b = barn = 1×10^{-24} cm^2

Table 5. Effect of interface scattering materials relative to wet ground

Nuclear reaction	Ratios for nuclear reaction at 1 m above various interface materials to that at 1 m above standard wet ground containing 30% moisture			
	Damp ground (15% moisture)	Dry ground (no moisture)	Concrete	Granite
$^{35}Cl(n,\gamma)^{36}Cl$	0.96	0.81	0.83	0.69
$^{151}Eu(n,\gamma)^{152}Eu$	0.97	0.85	0.87	0.74
$^{59}Co(n,\gamma)^{60}Co$	0.98	0.90	0.92	0.85
Neutron kerma	1.06	1.25	1.25	1.43
$^{63}Cu(n,p)^{63}Ni$	1.04	1.09	1.09	1.16
$^{32}S(n,p)^{32}P$	1.04	1.09	1.09	1.15

there was a 10% decrease in the secondary gamma-ray dose component directly under the Hiroshima burst. For Nagasaki, there was no difference under the burst, but at distance this dose component increased by 10%. These are negligible changes in the total gamma dose due to soil moisture content variations. These latter topics will be discussed in more detail in other chapters of this report.

Radiation Transport Calculations

The prompt radiation transport calculations were performed using both discrete ordinates and Monte Carlo methods. The discrete ordinates method was used to acquire energy and angular fluences from the transport of prompt neutrons and gamma rays leaking from the Hiroshima and Nagasaki bombs. These data were then combined with delayed radiation fluences and folded with activation and kerma response functions for comparing calculated and measured data. Monte Carlo calculations were used primarily to validate the discrete ordinates results, although some stand-alone calculations were also made using this methodology. The complete sequence of calculations that were performed to characterize the radiation environments at Hiroshima and Nagasaki is shown in Figure 1.

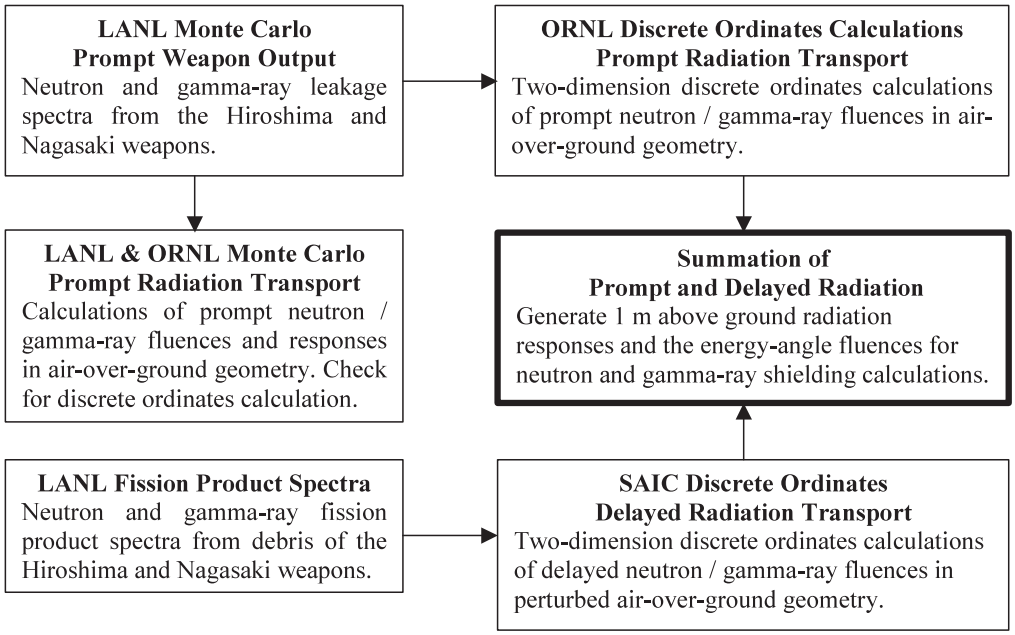

Figure 1. *Flow chart of the calculations.*

The weapon leakage calculations were performed at the Los Alamos National Laboratory (LANL) (Chapter 2) to obtain the neutron and gamma-ray leakage spectra and angular distributions from the Hiroshima and Nagasaki bombs. These data are the inputs to the discrete ordinates and Monte Carlo air-over-ground calculations. Spatial and angular dependent fluences calculated using the discrete ordinates methods were combined with delayed neutron and gamma-ray fluences for use in survivor shielding calculations.

Discrete Ordinates vs. Monte Carlo Transport

Two methods are most widely used for the accurate treatment of radiation transport in media: discrete ordinates and Monte Carlo. The discrete ordinates method uses equations to describe the radiation field that, when solved, yield the expected values of the fluence of particles throughout the problem geometry. Monte Carlo methods perform a simulation of source particle migration through the geometry media using random walk techniques. Both methods were employed to analyze the distribution of the Hiroshima and Nagasaki prompt neutrons and gamma rays.

The principal advantage of discrete ordinates transport is that the energy and angular distributions of the weapon neutrons and gamma rays are calculated at all mesh locations in the air-over-ground geometry model. A complete spatial picture of the radiation environment is obtained in a single calculation. Computer codes based on this method are available for assessing one-, two- and three-dimensional problems in rectangular, cylindrical or spherical geometry with an arbitrary number of energy groups.

Monte Carlo calculations, while capable of more accurate descriptions of problem

geometries, require additional computation efforts for each spatial location where particle fluences are to be computed. The statistical nature of the method can give rise to large uncertainties particularly where short mean free paths or the presence of highly attenuating media reduce the radiation particle population at points of interest. The problem is further compounded when the problem geometry descriptions contain large numbers of geometrical shapes or cells where the particle mean free paths are long compared to the cell dimensions. Having large numbers of these shapes at survivor distances will require very long running times to achieve statistically significant results throughout the calculation.

The discrete ordinates calculations can also provide the particle fluence on an arbitrary coupling surface surrounding a shielding geometry. These data can then be used with adjoint MASH Monte Carlo code system (Johnson 1999) to estimate the effectiveness of the particle fluence at that surface in causing a response in a detector within the shielding geometry. The particle fluence can be folded with a radiation dose or activation importance to obtain a desired response. This procedure was used to determine responses on and inside buildings and other structures at the two cities, and also to evaluate radiation doses to survivors who are shielded by terrain, houses, or other structures (Chapter 11).

Discrete Ordinates Calculations

A detailed synopsis of the mathematical basis for the discrete ordinates method can be found in Lathrop and Brinkley (1988) and Lewis and Miller (1993). Mynatt et al. (1969) also provide a comprehensive description of the mathematical development, applications and comparisons of discrete ordinates calculations with measurements.

The discrete ordinates method is a numerical integration technique that yields highly differential solutions to the Boltzmann transport equation. The technique derives its name from the replacement of the continuous angular variable by weighted values for discrete angles such that particles are only allowed to scatter along a finite number of directions rather than in all directions. The discrete representation of the spatial and energy variables in the discrete ordinates transport equation is obtained by dividing the geometry into a fine space mesh and by using multigroup cross sections.

ORNL used the DOORS Code System (DOORS3.2 1998) for the discrete ordinates transport calculations. The codes and calculational sequence used are shown schematically in Figure 2. Three essential items of information are needed before the calculations can be initiated; the description and composition of the air-over-ground environment, the weapon neutron and gamma-ray leakage spectra with angular distributions, and a coupled neutron and gamma-ray material multigroup transport cross-section library.

Neutron and Gamma-Ray Transport Cross Sections

The discrete ordinates calculations were performed using the ENDF/B-VI (Ver. 2) multigroup cross-section data described in the documentation of the Vitamin-B6 fine group neutron-gamma-ray cross-section library (Ingersoll et al. 1995). The library was constructed with 199 neutron and 42 gamma-ray energy groups. This was done to provide a pseudo-problem-independent cross-section database with sufficient detail in energy, temperature and resonance self shielding so as to

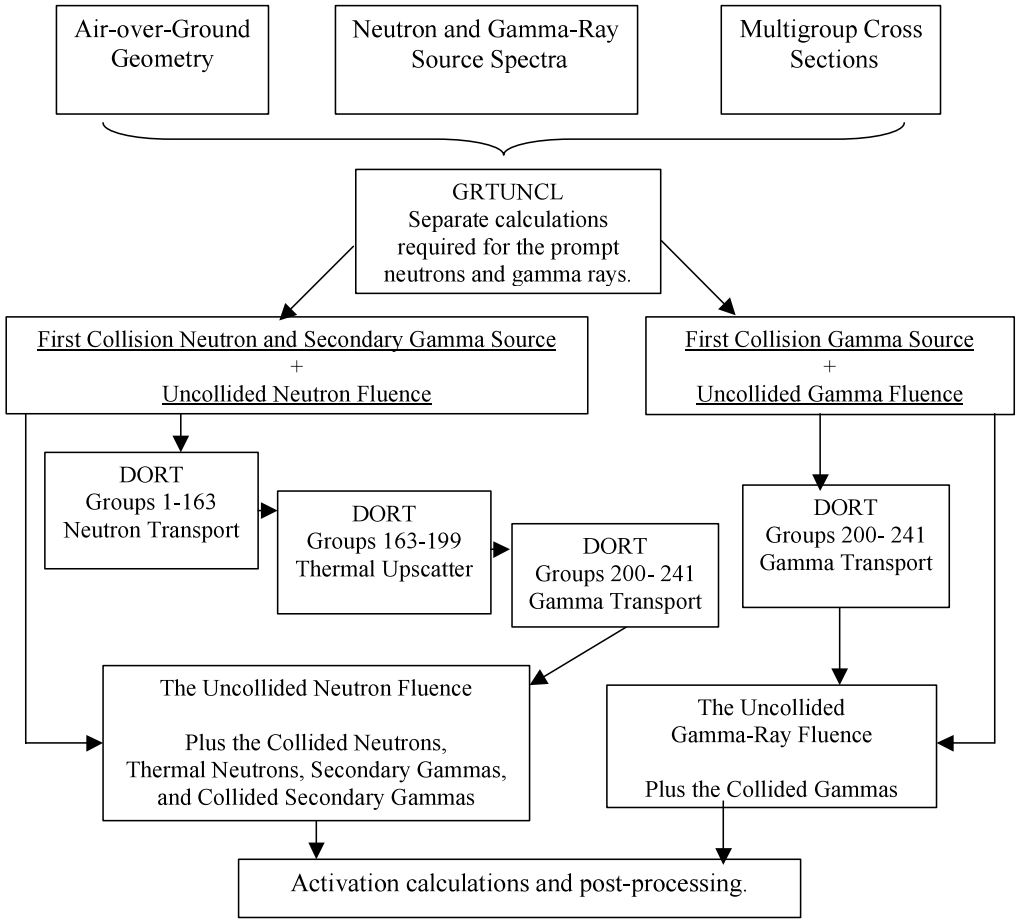

Figure 2. *Flow chart of the discrete ordinates calculations.*

be applicable to a wide range of problems, including the air-over-ground transport of fission weapon neutrons and gamma rays. The neutron and gamma-ray energy group structures are given in Appendix A. The expanded number of neutron and gamma-ray energy groups represents a considerable improvement over the 46-neutron, 22-gamma group structure used for the DS86 study and the 174-38 group structure in the Vitamin-E library used in the 1993 study by Rhoades et al. (1994).

In the neutron data, there are 36 thermal energy groups that include upscatter with 5.043 eV as the upper boundary. At higher energies, the group boundaries are almost identical with earlier VITAMIN libraries, which consist of a basic 100-group-mesh of equal lethargy width plus numerous additional boundaries to resolve resonance minima that are important in transport and shielding calculations.

The neutron weighting function used for these data is of the form typically chosen for fission reactor shielding problems. It consists of a smoothly varying combination of a Maxwellian thermal spectrum, E^{-1} slowing down spectrum, and a fission spectrum. The breakpoint energy

between the Maxwellian and E^{-1} shapes is 0.125 eV, and the breakpoint energy between the E^{-1} and fission shapes is 820.8 keV. The functional form of the weighting function is given by

Functional form	Energy limits	Groups
Maxwellian thermal spectrum (kt = 0.025 eV)		
$W_1(E) = C_1 E e^{-E/kT}$	10^{-5} eV to 0.125 eV	188-199
E^{-1} slowing down spectrum		
$W_2(E) = C_2/E$	0.125 eV to 820.8 keV	67-187
Fission spectrum (θ = 1.273 MeV)		
$W_3(E) = C_3 E^{1/2} e^{-E/\theta}$	820.8 keV to 20 MeV	1-66

where the continuous weighting spectrum is achieved with the following constants

$C_1 = 9{,}498.4\ eV^{-2}$; $C_2 = 1.0$; and $C_3 = 2.5625\ MeV^{-1.5}$.

The gamma-ray weighting function consists of an E^{-1} spectrum with a roll-off in the spectrum at lower energies to represent photoelectric absorption and a drop-off at higher energies corresponding to the Q-value for neutron capture.

The order of scattering in the Vitamin-B6 library for both neutrons and gamma rays is P_7 for nuclides with Z between 1 (hydrogen) and 29 (copper) and P_5 for the remainder (Z greater than for 29). The calculations were, however, carried out using P_3 scattering. Incorporating a higher order Legendre expansion in the transport calculations would have resulted in prohibitively large computer storage and memory requirements when the high order scattering data would be run with 241 energy groups, the large mesh required to describe the air-over-ground geometry and a high order angular quadrature. Using higher order scattering would only change the results by a few percent.

Neutron and Gamma-Ray Source Terms

The Hiroshima and Nagasaki neutron and gamma-ray leakage spectra were calculated by LANL in formats specifically tailored for input to the DOORS code. The neutron and gamma-ray leakage spectra were binned in energy intervals corresponding to the 200 neutron and 43 gamma-ray energy group structures, respectively. The bottom neutron group and bottom gamma leakage group were outside the range of the 199 neutron and 42 gamma-ray energy groups used in the air transport calculation. Otherwise there was an exact match in energy boundaries. There was no leakage in those two groups, and thus with this minor adjustment the bomb leakage spectra were prepared as the input for the air transport calculation. The results of the LANL calculations for the prompt radiations from the Hiroshima and Nagasaki bombs are discussed in Chapter 2.

The construction and materials used in the Hiroshima weapon result in an anisotropic distribution of the neutron and gamma-ray leakage. These data were binned into forty angular intervals corresponding to the polar intervals in the angular quadrature used in the discrete ordinates calculations. The full 240-angle quadrature is given in Appendix B. The radiation emission from the Nagasaki weapon is essentially isotropic.

Discrete Ordinates Air-over-Ground Geometry

The Hiroshima and Nagasaki air-over-ground environments were modeled in cylindrical R-Z geometry. The Z-axis was divided into 110 intervals that extended from 0.5 m below the ground to 2,000 m above the ground. The radius of the geometry extended out to 3,000 m in 130 mesh intervals. The left boundary of the R-axis was treated as a reflective boundary and the upper, lower and right (cylindrical surface) boundaries were void regions (i.e., particles reaching these surfaces escaped). The air was further divided into seven axial zones with air density varying as a function of altitude as shown in Table 3. The ground was modeled as a 50-cm-thick layer divided into 20 mesh intervals. A complete description of the air-over-ground geometry meshing is given in Appendix C. The energy-angle dependent sources were located on the axis of the cylinder at a height of burst (HOB) of 600 m for the Hiroshima bomb and 503 m for the Nagasaki bomb (Figure 3).

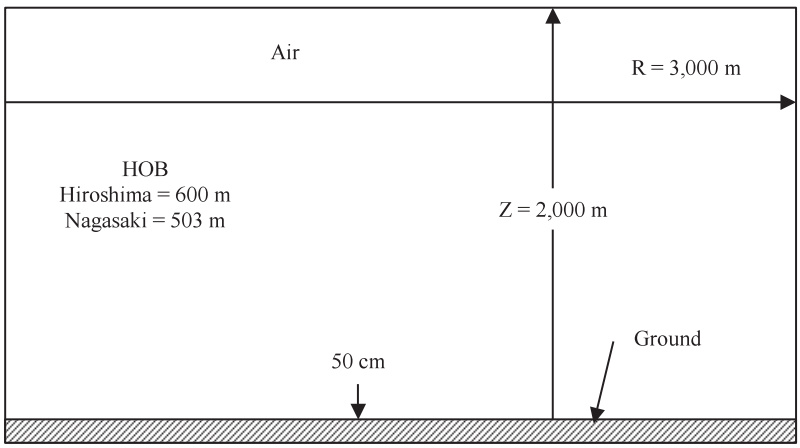

Figure 3. *Schematic of the air-over-ground model.*

Details of the Discrete Ordinates Calculations

In two-dimensional R-Z geometry, the finite number of angles may result in an anomaly called “ray effects”. The problems in which ray effects are observed are those where the source and detectors are small compared to the total geometry and the scattering mean free path is long compared to the space mesh. If a problem such as a point source or a point detector in a low scattering medium is approximated by the discrete ordinates differences equations, the particle fluences along a spherical surface centered about the source are observed to rise and fall in a wave-like pattern instead of being constant. The peaks in the distribution fall along rays following the polar angles of the quadrature centered about the source.

In the discrete ordinates solution of the two-dimensional cylindrical transport equation, the angles in the quadrature are arranged in levels that are comprised of directions having the same polar direction cosine, η. Within these levels, particles change direction from both the curvature and scattering derivatives. Transfers from a direction in one η level to one in another level occur only from scattering. If the source region is distributed or dominant, no ray effects appear. On the

other hand, if the source is localized and spatial convection is dominant (i.e., the change in particle fluence is governed by geometric attenuation), ray effects can be significant.

One way to mitigate ray effects is to increase the number of η levels. This approach is generally uneconomical and usually not effective. The more optimum solution is to use an analytic first collision source. The discrete-ordinates calculations were carried out in several steps (Figure 2). The GRTUNCL code (DOORS3.2 1998) was used initially to obtain the uncollided neutron fluence and first collision sources throughout the geometry mesh. The problem geometry is described with the same mesh and material zones used in the DORT model. The uncollided fluence is calculated for every mesh point and for every energy group, and the first collision source is written for each radial and axial interval and energy group. GRTUNCL was written to handle both isotropic and anisotropic source distributions.

The first collision distributions were input to the DORT code (DOORS3.2 1998). DORT was then run in four steps:

1) to obtain the collided fluence for neutron energy groups 1 through 163,
2) to generate the fluence distributions from thermal neutron up-scattering in neutron energy groups 163 through 199,
3) to account for the secondary gamma-ray fluences resulting from prompt (n,γ) reactions in the air and ground, and
4) to transport the prompt gamma-ray leakage from the weapon.

DORT was run to achieve 10^{-3} convergence in the collided fluence for all neutron and gamma-ray energy groups.

At the completion of the DORT transport sequences, the uncollided- and collided-neutron and gamma-ray fluences were summed to obtain the total fluence distributions for the event. The VISTA code (DOORS3.2 1998) was used to format the GRTUNCL-DORT data for use in a forward-adjoint processes. The prompt and delayed radiation were combined in this format and used to perform terrain, house, and other shielding calculations.

The transport, cross-section data, and source description used in the discrete ordinates calculations performed here differ from those used in previous studies. The differences between the DS86 and DS02 calculations are summarized in Table 6.

Results of Discrete Ordinates Calculations - Hiroshima Weapon

The principal purpose of the prompt and delayed radiation calculational effort is to substantiate the radiation doses received by survivors at Hiroshima and Nagasaki. Comparisons of measured and calculated activation data are made to validate the radiation transport codes and cross-section data that are the basis for the estimation of the radiation doses to survivors.

The calculations for the prompt radiation from the Hiroshima bomb were performed for a 600-m HOB. Contours of the calculated total neutron and secondary gamma-ray fluences are shown in Figures 4 and 5. The data are given as a function of ground range and height above the ground plane and are normalized to a weapon yield of 1 kt. Also indicated in the figures are the seven altitude intervals into which the air was divided to account for the dependence of the air density with altitude shown in Table 3.

In the Hiroshima air-over-ground R-Z geometry, the source and detector regions are small compared to the geometry, and the scattering mean free path is large compared with the space meshing. In this geometric representation, ray effects can occur. However, the fluence profiles

Table 6. Comparison of DS86 and DS02 discrete ordinates parameters

DS86	DS02
Transport Calculations	
DOT-4 2-D Discrete Ordinates	DORT 2-D Discrete Ordinates
First Collision Source	First Collision Source
240-Direction Angular Quadrature	240-Direction Angular Quadrature
Negative Source Fix up	No Negative Source Fix up
Convergence Criterion 1×10^{-2}	Convergence Criterion 1×10^{-3}
Weighted-Difference Fluence Calculation	Theta-Weighted Fluence Calculation
Source Term	
LANL 1983 27 Neutron and 20 Gamma-Ray Energy Groups	LANL 2000 199 Neutron and 43 Gamma-Ray Energy Groups
20 Angular Bins	40 Angular Bins
Geometry	
Seven-Zone Air Density Profile	DS86 Material Compositions and Profiles with Continuous Vertical Density Variation
Maximum Radius 2,800 m	Maximum Radius 3,000 m
Maximum Height 1,500 m	Maximum Height 2,000 m
Maximum Radial Mesh 25 m	Maximum Radial Mesh 25 m
Cross Sections	
ENDF/B-V	ENDF/B-VI (Ver. 2.0)
46 Neutron Energy Groups	199 Neutron Energy Groups
22 Gamma-Ray Energy Groups	42 Gamma-Ray Energy Groups
P_3 Scattering (custom weighted by region)	P_3 Scattering (custom weighted by region)

shown in Figures 4 and 5 vary smoothly with distance and altitude. The absence of rays shows the importance of initiating the calculations with GRTUNCL to compute the uncollided fluence and first collision source. It is interesting to note that the secondary-gamma-ray contours shown in Figure 5 are also free of ray effects. These gamma rays are produced from the reactions of neutrons with the air and ground and are transported using the DORT code with no initial GRTUNCL calculation. The prompt gamma rays that are initially transported using GRTUNCL are also essentially free of ray effects. Incorporation of the fine energy group cross sections further mitigates ray effects in the calculated radiation environment. Both were adopted in this work.

Figures 6 through 8 compare the prompt neutron and prompt gamma-ray fluence per unit lethargy at 1 m above the ground as a function of energy and slant range. The fluence, φ_L, in each lethargy interval was obtained using the relation:

$$\varphi_L = \varphi_g / \ln(E_{gu}/E_{gl}) ,$$

where E_{gu} and E_{gl} are the upper and lower energy bounds of the neutron or gamma-ray fluence in energy group g.

The spectra continually approach equilibrium with increasing range. The sharp peaks in the gamma-ray spectra at 511 keV seen in Figures 7 and 8 are due to the pair production by gamma rays. Also evident in the secondary gamma-ray spectra of Figure 7 are the 2.3-MeV gamma-ray peak from neutron capture in hydrogen. The peaks at higher energies arise from thermal neutron capture reactions in the air and ground.

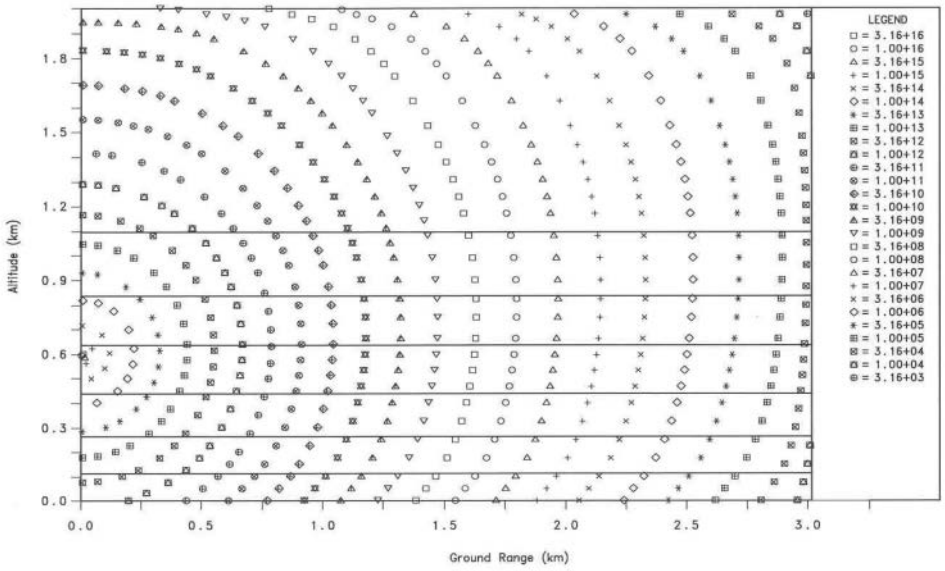

Figure 4. *Contours of constant prompt neutron fluence (Hiroshima bomb).*

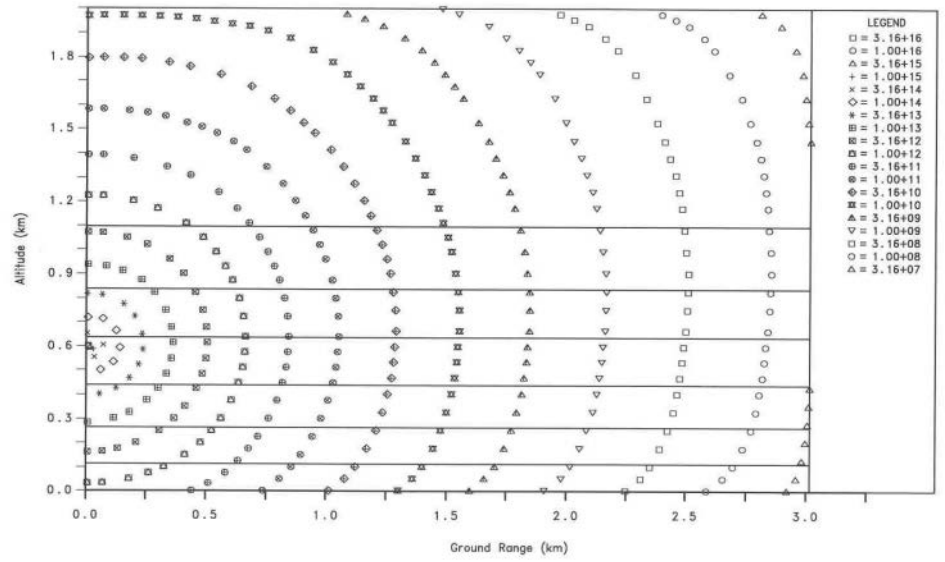

Figure 5. *Contours of constant prompt secondary gamma-ray fluence (Hiroshima bomb).*

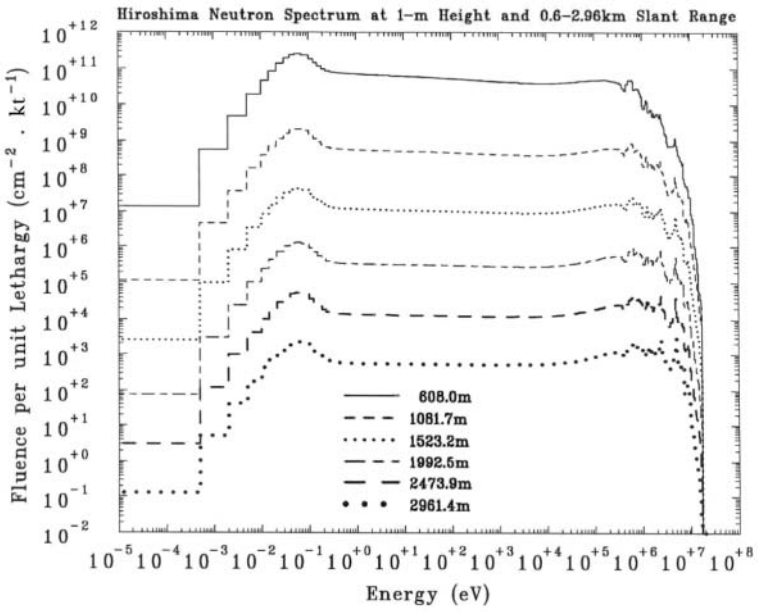

Figure 6. *Prompt neutron fluence per unit lethargy vs. neutron energy as a function of slant range (Hiroshima bomb).*

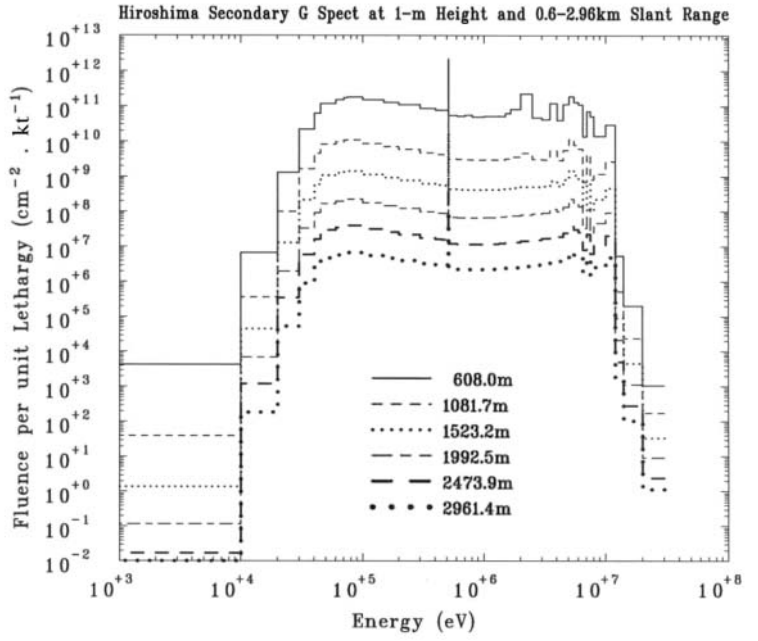

Figure 7. *Secondary gamma-ray fluence per unit lethargy vs. gamma-ray energy as a function of slant range (Hiroshima bomb).*

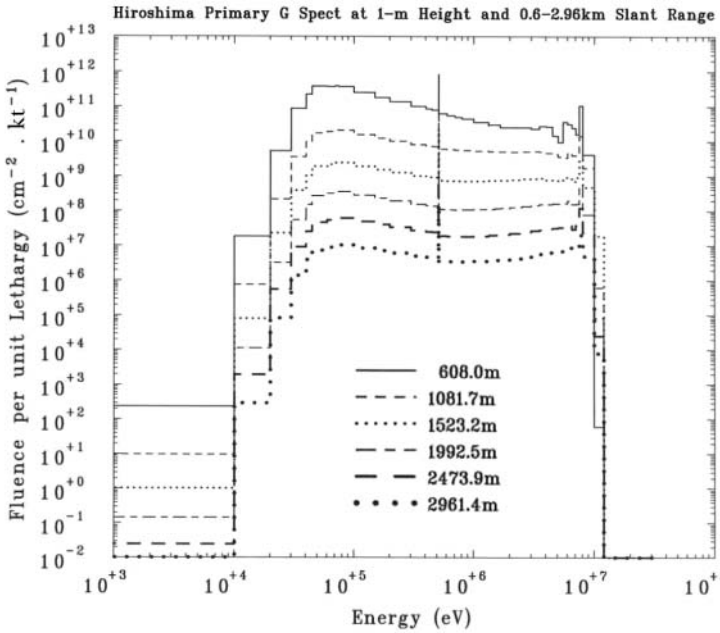

Figure 8. *Prompt gamma-ray fluence per unit lethargy vs. gamma-ray energy as a function of slant range (Hiroshima bomb).*

Figure 9 shows the number of fast neutron (n,p) reactions in ^{32}S and ^{63}Cu. These data were calculated at 1 m above the ground and are plotted as a function of slant range. The data, normalized to a weapon yield of 1 kt, were obtained by folding the prompt neutron fluence with the activation response functions shown in Figure 10. The response functions were obtained by converting ENDF/B-VI (n,p) cross sections to units of (reactions/cm^2)/(neutron-gram of material). The effective threshold for the $^{32}S(n,p)$ reaction is approximately 2.5 MeV and that for the $^{63}Cu(n,p)$ reaction is approximately 1.4 MeV.

Figure 11 shows the number of (n,γ) reactions per microgram of ^{59}Co, ^{35}Cl and ^{151}Eu at 1 m above the ground as a function of slant range. These data are also normalized to a weapon yield of 1 kt. These data were also obtained by folding the neutron fluence with the ^{59}Co-, ^{35}Cl- and ^{151}Eu-(n,γ) response functions shown in Figure 12. In order to coplot ^{59}Co and ^{35}Cl it was necessary to reduce the ^{35}Cl by 10.

Activation of ^{59}Co, ^{35}Cl and ^{151}Eu is due chiefly to thermal and epithermal neutron capture reactions. This can be seen in Figure 13, which shows the energy integrated $^{151}Eu(n,\gamma)^{152}Eu$ activation at 1 m above the ground plotted as a function of neutron energy (the lower boundary of the energy group is used for the integration). Data are given for several slant range distances. Note that each curve is normalized differently so that their spectral response can be compared. Ninety percent of the activation of ^{151}Eu is due to reactions of neutrons with energies below about 0.1 eV. The jump in the activation at about 0.5 eV is due to the resonance peak in the response function for ^{151}Eu shown in Figure 12. The energy integrated activation curves for ^{59}Co and ^{35}Cl show essentially the same behavior with approximately ninety percent of the activation occurring at neutron energies below about 0.1 eV.

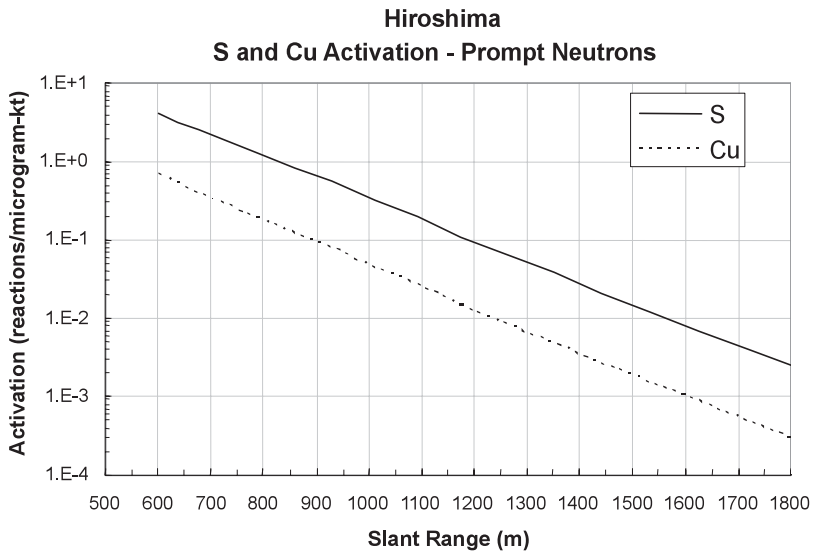

Figure 9. *Activation of S and Cu by prompt neutrons vs. slant range (Hiroshima bomb).*

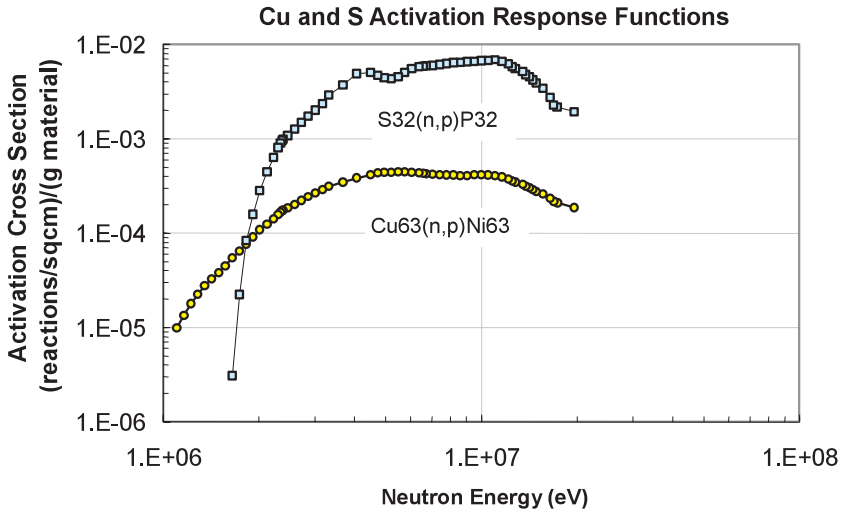

Figure 10. *S and Cu activation response functions vs. neutron energy [response functions are given in (reactions/cm^2)/(gram material-kt)].*

Next Page